Thermoelectric performance of n-type Bi_2S_3-alloyed $Bi_2Te_{2.7}Se_{0.3}$

Raphael Fortulan [a,b], Adam Brown [a], Illia Serhiienko [c,d], Takao Mori [c,d], Sima Aminorroya Yamini [a,e,*]

[a] *Materials and Engineering Research Institute, Sheffield Hallam University, Sheffield, UK*
[b] *Unconventional Computing Laboratory, University of the West of England, Bristol, UK*
[c] *International Center for Materials Nanoarchitectonics (WPI-MANA), National Institute for Materials Science, Tsukuba, Japan*
[d] *Graduate School of Pure and Applied Science, University of Tsukuba, Tsukuba, Japan*
[e] *School of Aerospace, Mechanical and Mechatronic Engineering, The University of Sydney, Sydney, 2006, Australia*

ARTICLE INFO

ABSTRACT

The effect of isovalent sulfur substitution on the thermoelectric properties of n-type $Bi_2Te_{2.7}Se_{0.3}$ alloy has been studied systematically. At low sulfur concentrations, where the samples are single phase, changes in defect chemistry and density of states impacted significantly electrical resistivity and thermopower. Isovalent sulfur substitution enhanced thermopower and reduced thermal conductivity for both single and multiphase samples. This reduction in thermal conductivity was particularly noticeable in samples containing Bi_2S_3-based secondary phase, reaching a low thermal conductivity of ~0.3 W m^{-1} K^{-1} at 525 K. A maximum figure of merit, zT, of 0.55 was achieved for the sample with the highest sulfur content, demonstrating the potential of this approach to optimise the thermoelectric performance of Bi_2Te_3-based materials.

1. Introduction

Alloys of chalcogenides (Te and Se) and pnictogenides (Bi and Sb) have shown the best performance for low-temperature range power generation [1–3]. In particular, binary p-type and n-type compounds are the best-performing thermoelectric materials at around room temperature [4–10]. The presence of Se at Te sites creates donor levels that increases the carrier concentration, and alloying decreases the thermal conductivity [11,12]. The anisotropy of the layered crystal structure also plays an important role in its efficiency [13,14].

The addition of dopants such as Cl [15], Cu [16], Zn [17], I [18], and CuI [19] has been shown to improve the power factor of $Bi_2Te_{2.7}Se_{0.3}$, while nano-precipitates have been proposed to decrease the thermal conductivity and increase thermoelectric efficiency (zT). Recently, there has been great interest in the isovalent substitution of sulfur for Te sites in p-type [20,21] and n-type [2,22] bismuth telluride alloys. Sulfur affects the naturally occurring antisites and Te vacancies, increasing the carrier concentration of these alloys [2]. Isovalent sulfur doping has enhanced both the thermopower and electrical conductivity of Bi_2Te_2Se through modification of the conduction band of this compound, which is very sensitive to spin-orbit splitting [23], and increased effective mass [24]. The formation of secondary phases owing to the addition of sulfur

[25,26] resulted in a decrease in thermal conductivity by introducing multiscale scattering of phonons [26].

Here, we have systematically investigated the effect of Bi_2S_3 alloying on the thermoelectric properties of n-type doped $Bi_2Te_{2.7}Se_{0.3}$ compound. Unlike previous studies that focused either on light sulfur doping or on the effect of secondary phases on the transport properties of the compound [2,22], our work systematically explores a wide range of sulfur concentrations, covering both regimes. At low sulfur concentrations, changes in the density of states and defect chemistry significantly altered electrical resistivity and thermopower. At higher sulfur concentrations, above 2.5 %, a Bi_2S_3-based secondary phase formed in the matrix, remarkably effective at reducing thermal conductivity, approaching theoretical minimum values. This approach allows us to investigate the transition from single-phase to multiphase systems and their impact on thermoelectric properties. Our study is motivated by the potential of sulfur to simultaneously modify the electronic structure at low concentrations and introduce beneficial microstructural changes at higher concentrations. These findings highlight promising strategies to engineer high-performance n-type Bi_2Te_3-based thermoelectric materials.

* Corresponding author. School of Aerospace, Mechanical and Mechatronic Engineering, The University of Sydney, Sydney, 2006, Australia.
E-mail address: s.aminorroaya@sydney.edu.au (S. Aminorroaya Yamini).

2. Experiments

2.1. Samples fabrication

High purity elements of bismuth shots (Bi, 99.999 %, Alfa Aesar), tellurium chunks (Te, 99.999 %, Alfa Aesar), selenium shots (Se, 99.999 %, Alfa Aesar), and sulfur pieces (S, 99.99 %, Alfa Aesar) were weighted according to the stoichiometry of $Bi_{2-y/3}Cr_{y/3}[(Te_{2.7}Se_{0.3})_{1-x}S_x]_{1-y}Cl_y$ where $x = (0, 0.003, 0.008, 0.025, 0.05,$ and $0.2)$ and $y = 0.005$. All samples are doped with the same concentration of $CrCl_3$ to increase the charge carrier concentration; for simplification, they are referred to as $Bi_2Te_{2.7}Se_{0.3} - xBi_2S_3$ throughout the text. Raw elements were loaded into vacuum-sealed quartz ampules in an inert atmosphere glove box and sealed under vacuum. The ampules were heated to 850 °C, held at this temperature for 12 h, quenched in cold water, and annealed at 450 °C for 72 h. The resulting ingots were then ground by hand into fine powders in an agate mortar and pestle in a glove box and sintered under vacuum to produce 11 mm diameter rods using spark plasma sintering (SPS) technique (KCE FCT-H HP D-25 SD, FCT Systeme GmbH, Rauenstein, Germany) at a pressure of 50 MPa and a temperature of 400 C for 4 min. The densities of all samples were measured from the dimensions and weight of the rods. The average density of the samples was approximately 89 % of their theoretical density (see Table S1 for more details). The samples exhibited a high ratio of porosity due to the low actual force applied by the SPS equipment, resulting in an effective pressure lower than the set one and consequently samples of lower density.

2.2. Materials characterization

Powder X-ray Diffraction (PXRD) measurements were conducted on a PANalytical X'Pert Pro diffractometer with Cu–K α 1 radiation ($\lambda = 0.15406$ nm, 40 kV, 40 mA). The lattice parameters and quantitative phase percentages were determined by the Rietveld refinement method using the GSAS-II software [27].

2.3. Thermoelectric transport properties

Simultaneous measurements of electrical resistivity and thermopower were conducted on an LSR-3 (Linseis) system. Thermal conductivity was calculated as $\kappa = D \cdot c_p \cdot d$, where $D, c_p,$ and d are the thermal diffusivity, specific heat capacity, and density, respectively. Thermal diffusivity was measured by the laser flash analysis (LFA) method using an LFA 467 HyperFlash, Netzsch. The specific heat capacity was determined using a differential scanning calorimeter (DSC 8000, PerkinElmer) using the sapphire standard method (ASTM Standard E1269 [28]).

The room temperature Hall coefficient (R_H) measurement was carried out on an ECOPIA 3000 Hall Effect Measurement System with a magnetic field of 0.55 T.

The longitudinal speed of sound was measured using the pulse-echo method at room temperature via an ultrasonic thickness gauge (38DL PLUS, Olympus).

3. results and discussion

3.1. Structural and phase analysis

The PXRD patterns of $Bi_2Te_{2.7}Se_{0.3} - xBi_2S_3$, $x = (0, 0.003, 0.008, 0.025, 0.05,$ and $0.2)$ are shown in Fig. 1. All samples showed a $Bi_2Te_{2.7}Se_{0.3}$ hexagonal primary phase (space group R$\overline{3}$m, PDF Card #050–0954), and samples with $x > 0.025$ contained an orthorhombic crystal structure of Bi_2S_3 secondary phase (space group $Pnma$, PDF Card #04-014-6675). The estimated phase composition, lattice parameters, and crystallite size are given in Table 1 The small peaks for the
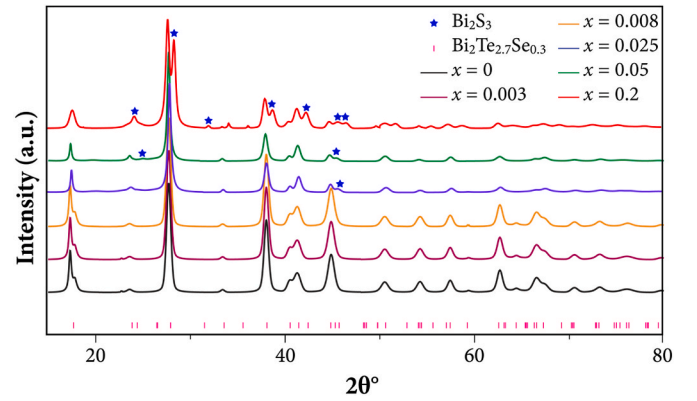

Fig. 1. Powder X-ray diffraction patterns of $Bi_2Te_{2.7}Se_{0.3} + xBi_2S_3$ $x = (0, 0.003, 0.008, 0.025, 0.05,$ and $0.2)$. Peaks of Bi_2S_3 are marked with a blue star (★).

secondary presented in the diffraction patterns of $x = 0.025$ and 0.05 do not allow for an accurate estimate of the crystallite size of the samples, so they are not reported here.

3.2. Electronic transport properties

The temperature dependence of electrical resistivity (ρ), thermopower (α), and thermal conductivity (κ) was measured at the perpendicular (in-plane) direction relative to the sintering pressure. Fig. 2(a)–(d) show, respectively, the electrical resistivity, thermopower, power factor (PF, α^2/ρ), and thermal conductivity of $Bi_2Te_{2.7}Se_{0.3} - xBi_2S_3$, $x = (0, 0.003, 0.008, 0.025, 0.05,$ and $0.2)$ samples. The electrical resistivity of the single-phase samples $x = 0$ and 0.003 (Fig. 2(a)) shows intrinsic semiconductor behavior with values decreasing with temperature [29]. The electrical resistivity of the multiphase samples with $x = 0.025$ and 0.05 shows the intrinsic behavior as well, whereas the electrical resistivity of the sample with $x = 0.2$ shows a weak metallic behavior with a small positive slope of dρ/dT. The low charge carrier concentrations (Table 2) explain the exhibited intrinsic behavior of these samples.

The addition of sulfur to the samples increases the electrical resistivity of the samples at concentrations of $x = 0.003, 0.008, 0.025,$ and 0.05.

The resistivity values reported here are higher than those found in the literature for $Bi_2Te_{2.7}Se_{0.3}$ [30,31], but similar to those observed in porous samples [32]. Our sintered samples exhibited a relative density of approximately 89 %, indicating a significant level of porosity. This high porosity plays a crucial role in scattering charge carriers, which in turn reduces their mobility and increase the electrical resistivity [33].

Hall effect measurements were performed at 300 K to measure the Hall coefficient of the samples and to evaluate their Hall carrier concentration ($n_H = 1/(R_H \cdot e)$) and mobility ($\mu_H = R_H/\rho$), as shown in Table 2. The charge carrier concentration of single-phase alloys ($x = 0, 0.003$ and 0.008) has increased slightly by alloying; however, the carrier concentration variation of multiphase compounds shows no specific trend. The observed changes in the carrier concentration of the sulfur-alloyed samples can be explained by the defect control in the system. Bismuth telluride alloys typically exhibit three major atomic defects [16]: (a) antisite defects of Bi at Te sites (Bi'_{Te}, which contributes one hole per defect); (b) vacancies at Te sites ($V_{Te}^{\cdot\cdot}$, which contributes two electrons per defect); (c) and vacancies at Bi sites (V_{Bi}''', which contributes three holes per defect) [34,35] (represented using the Kröger-Vink notation [36]). The addition of selenium in these alloys tends to increase the number of vacancies in Te ($V_{Te}^{\cdot\cdot}$) and Se ($V_{Se}^{\cdot\cdot}$) since the enthalpy of evaporation of Se (95.48 kJ mol^{-1} [37]) and Te (114.1 kJ mol^{-1} [37]) is much lower than that of Bi (178.632 kJ mol^{-1} [38]); this increases the carrier concentration of electrons and contributes to the n-type behavior

Table 1

Phase analysis of $Bi_2Te_{2.7}Se_{0.3} + xBi_2S_3$, x = (0, 0.003, 0.008, 0.025, 0.05, and 0.2) obtained from the Rietveld refinement of the powder X-ray diffraction patterns.

			$Bi_2Te_{2.7}Se_{0.3}$			Bi_2S_3		
x	. a = b (Å)	c (Å)	D (μm)	wt. %	a (Å)	b (Å)	c (Å)	D (μm)
0	4.3605(5)	30.2661(19)	0.52	...	...	...	...	...
0.003	4.3751(4)	30.3880(18)	0.57	...	...	...	...	...
0.008	43844(7)	30.2565(28)	0.53	...	...	...	...	...
0.025	4 3492(3)	30.3002(22)	0.6	5.1(4)	11.505(13)	4090(5)	11.142(15)	...
0.05	4.3600(29)	30.153(15)	0.65	11.6(16)	11.446(30)	4.159(12)	10.687(21)	...
0.2	4.3733(7)	30.416(5)	0.59	23.0(4)	11.239(10)	4.0609(15)	11.492(8)	0.58
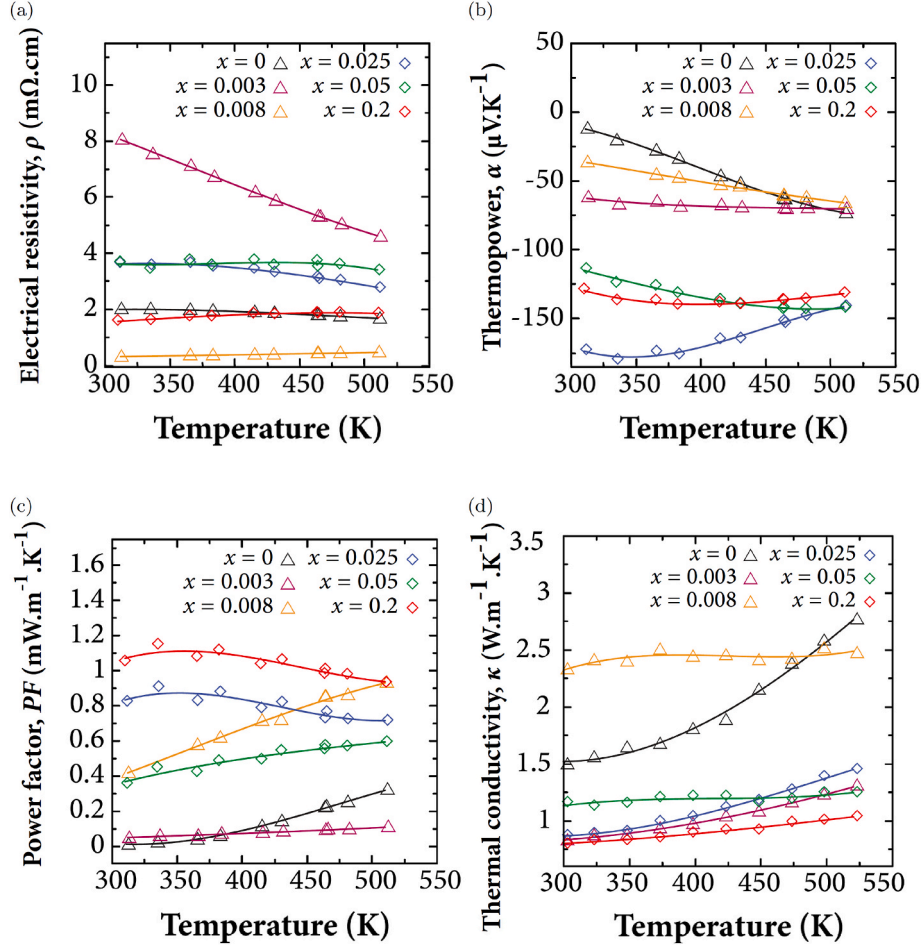
Fig. 2. Temperature dependence of the (a) electrical resistivity, (b) thermopower, (c) power factor, and (d) thermal conductivity of $Bi_2Te_{2.7}Se_{0.3} - xBi_2S_3$, x = (0, 0.003, 0.008, 0.025, 0.05, and 0.2) samples.

Table 2

Hall carrier concentrations and mobility of $Bi_2Te_{2.7}Se_{0.3} + xBi_2S_3$, x = (0, 0.003, 0.008, 0.025, 0.05, and 0.2) samples.

X	n_H ($\times 10^{19}$ cm^{-3})	μ_H (cm^2 V^{-1} s^{-1})
0	1.57	224.0
0.003	2.74	81.19
0.008	2.58	131.0
0.025	1.42	76.75
0.05	1.88	73.06
0.2	7.73	47.55

of these materials with high carrier concentrations [39,40]. The low value of the thermopower (Fig. 2(b)) for the sample with $x = 0$ at room temperature (~ -12.5 μV K^{-1}) indicates that vacancy of Te and Se is not the most prevalent mechanism in our samples, but most likely antisite

defects are responsible for the changes in carrier concentration of single phase samples in our study [20,41]. For the single-phase samples, the charge carrier concentration increases with the concentration of sulfur, most likely due to increased sulfur vacancies because of easy evaporation of sulfur. However, the mechanism is different for the multiphase samples. The carrier concentration of multiphase samples ($0.025 \leq x \leq 0.2$) can be described by sulfur defects ($V_S^{..}$), which contributes to two electrons per defect. This sulfur vacancy in the sulfur-rich secondary phase appears to balanced out the reduction (fractional) of the electron-donating defects present in the $Bi_2Te_{2.7}Se_{0.3}$ phase, maintaining a relatively constant carrier concentration. Meanwhile, the unique electronic behavior of the sample with $x = 0.2$ suggests that high-energy donors are accessible from the conduction band of the matrix and contribute to the electronic conduction of this sample. A possible explanation for this effect is that the interface between the two phases forms an intermediate band of impurity states [42,43].

The single-phase sample ($x = 0$) shows a carrier concentration of 1.57×10^{19} cm^{-3} and carrier mobility of 224 cm^2 V^{-1} s^{-1} at 300 K. The Hall carrier mobility of samples decreases with the increase in sulfur content, reaching the lowest value of 47.55 cm^2 V^{-1} s^{-1} for the multi-phase sample $x = 0.2$; most likely due to the increased scattering at the interfaces between phases. On the other hand, the carrier concentration shows the opposite trend to the resistivity, with its maximum value of 7.73×10^{19} cm^{-3} for the sample with the highest concentration of secondary phase ($x = 0.2$). This dependence of the carrier concentration and mobility on the sulfur concentration indicates that the reduction in electrical conductivity is due to the decrease in carrier mobility, while the significant improvement for $x = 0.2$ is due to the increase in carrier concentration.

The thermopower for all samples has negative values at room temperature, indicating *n*-type conduction (Fig. 2(b)). The linear dependence of thermopower to temperature up to 350 K for all samples indicates that at this temperature range, the main parameter effects on thermopower is the thermal diffusion of electrons, as predicted by Mott's formula [44]. This linear relationship between thermopower and temperature is observed over the whole measured temperature range for sulfur-free and lightly alloyed samples ($x = 0$, 0.003, and 0.008).

It is well known that the thermopower is strongly dependent on the band structure and the density of states (DOS) around the Fermi level (E_F) [45]. Given the high sensitivity of the thermopower values to the sulfur concentration, it can be inferred that the presence of sulfur in these samples significantly changes the DOS around E_F. This significant dependence of the DOS on sulfur content was previously observed in a

Bi$_{0.5}$Sb$_{1.5}$Te$_3$ alloy [41]. The magnitude of the thermopower for samples with added sulfur was generally higher than that of the sample without sulfur. (~-12.5 µV K^{-1}) and ranged from ~-46.8 µV K^{-1} for the sample with $x = 0.008$ to ~-173.9 µV K^{-1} for the sample with $x = 0.025$.

Multiphase samples of $x = 0.025$, 0.05, and 0.2 have the highest values of α, comparable to those found in the literature [19], and presented nonlinear behavior at high temperatures, exhibiting bipolar conduction [46]. The presence of additional phases in a material with highly mismatched band structures can introduce the energy filtering effect, screening out low energy carriers using a potential barrier that is proportional to the difference in electron affinity of the materials, resulting in an increased thermopower of the bulk material [47]. Considering the low values of α for the sulfur-free sample, the power factor of all samples with added sulfur is higher than that of the sulfur-free sample (Fig. 2(c)). The combination of low resistivity and relatively high thermopower of the sample with $x = 0.02$ resulted in the highest *PF* for this sample.

In general, the thermal conductivity of the sulfur-containing samples is lower than that of the single-phase sulfur-free sample, except for the sample with $x = 0.008$ (Fig. 2(d)).

To understand the contribution of phonons and both majority and minority carriers to the heat transport mechanisms in the materials, the two-band model, described in the Supporting Information, was used to evaluate the lattice thermal conductivity of these samples. Measured thermopowers, carrier concentrations, and electrical resistivities were used to estimate the density of state effective mass, m^*_{DOS}, for both holes and electrons, the deformation potential, E_{def}, of the conduction and
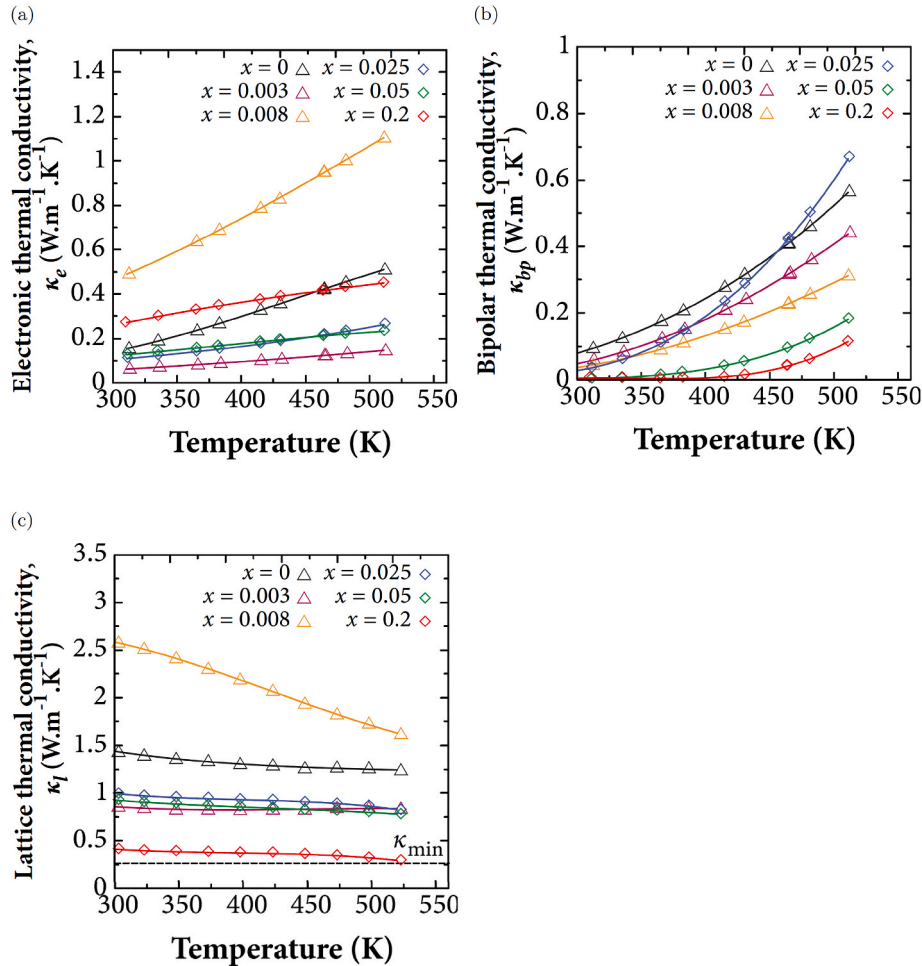

Fig. 3. Temperature dependence of the (a) electronic, (b) bipolar, and (c) lattice thermal conductivities (estimated from the two-band model and the Wiedemann-Franz law; detailed in the SI) of Bi$_2$Te$_{2.7}$Se$_{0.3}$ − xBi$_2$S$_3$, $x =$ (0, 0.003, 0.008, 0.025, 0.05, and 0.2).

valence bands, and the reduced Fermi level. The fitted values for the multiband model are provided in the Supporting Information.

The calculated values of the electronic, bipolar, and lattice contributions to the total thermal conductivity of samples are shown in Fig. 3 (a)–(c), respectively.

The electronic thermal conductivity, κ_e, follows the same behavior of the electrical resistivity, with the low resistivity samples showing higher values of electronic thermal conductivity. The bipolar thermal conductivity values show an exponential increase with temperature due to the thermal activation of minority carriers [46]. The presence of sulfur reduced the values of κ_{bp}, with the lowest values for the samples with high concentrations of sulfur up to ~ 450 K, possibly due to the presence of additional majority carriers in these materials. Care must be taken in interpreting these results, as these models assume samples as single-phase alloys, while many thermoelectric materials, including some compounds of the current study, contain a substantial ratio of secondary phases.

The lattice thermal conductivity of sulfur alloyed samples decreased significantly compared to the single-phase sulfur-free sample, except for the sample with $x = 0.008$. It is worth noting that this sample has a higher relative density (~ 95 %) than other samples (See Table S1 for detailed densities), resulting in a much higher electrical conductivity (Fig. 2(a)) and consequently electronic contribution to the total thermal conductivity (Fig. 3(a)) of this sample relative to others. This has therefore resulted to apparent higher lattice thermal conductivity for this sample in Fig. 3(c).

The multiphase sample with the highest sulfur concentration and the largest proportion of secondary phase, $x = 0.2$, had a surprisingly low value of κ_l, approaching Clarke's limit [48] of $\kappa_{min} \approx 0.261$ W m^{-1} K^{-1} for Bi$_2$Te$_3$ at higher temperatures. The behavior of κ_l is mainly determined by the phonon-scattering mechanisms that occur in the materials, including phonon-phonon normal/Umklapp process scattering, boundary scattering, and pore scattering [49]. The remarkably low values of lattice thermal conductivity in these samples are attributed to: the relatively high porosity values due to the low density of the sintered samples, which created additional scattering centers [50,51]; and the presence of a secondary phase, which created additional boundary scattering.

3.3. Figure of merit, zT

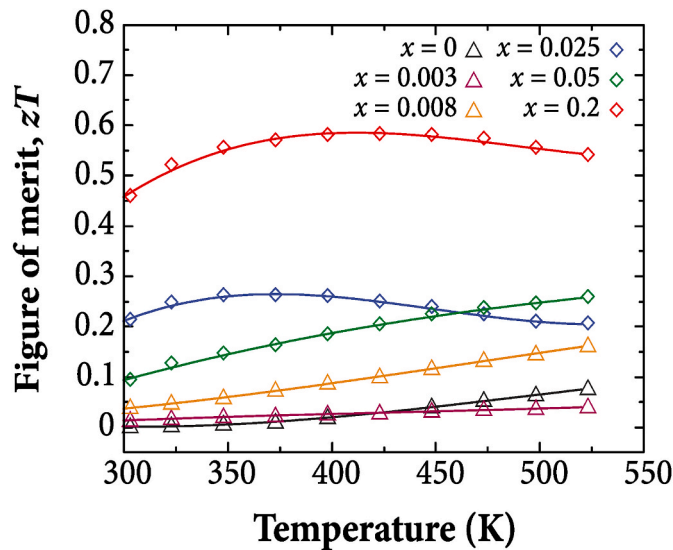The temperature dependence of the thermoelectric figure of merit

(zT) for samples of Bi$_2$Te$_{2.7}$Se$_{0.3}$ − xBi$_2$S$_3$, $x = $ (0, 0.003, 0.008, 0.025, 0.05, and 0.2), are shown in Fig. 4.

The zT values of sulfur-added Bi$_2$Te$_{2.7}$Se$_{0.3}$ samples increase significantly compared to sulfur-free samples. Notably, the maximum zT value of approximately 0.55 is achieved for the sample with $x = 0.2$. This enhancement in zT is attributed to the concurrent improvement in the thermopower and a reduction in the thermal conductivity. Despite considerable improvement of zT values for sulfur-added samples compared to sulfur-free compound, the zT value of our samples remain relatively low compared to the samples with similar compositions reported in the literature that reached zT of up to 1.2 [16,30,52–59]. Although, we are confident that low efficiency of our samples is due to their low relative density, we have compared the efficiency of our best sample with the literature, using a raincloud plot of zT values for Bi$_2$Te$_{2.7}$Se$_{0.3}$-based compounds at temperatures of 300 K, 400 K, and 500 K (Fig. 5). These values were obtained from an open database for materials, Starrydata [60], using a Python API. The plot includes values of our Bi$_2$Te$_{2.7}$Se$_{0.3}$ + 0.2 at.% Bi$_2$S$_3$ sample.

The zT values of our sample is located at the minimum values of the dataset at room temperature and increases towards the lower quartile of the data at higher temperatures of 400 K and 500 K. Notably, the distribution of zT values in the literature are heavy tailed with a large spread of values, specifically at 400K, indicating that our data is not an outlier. Although the average zT values show an upward trend from room temperature and reduction at 500K, the efficiency of our sample remained relatively constant over the measured temperature range.

The primary factor contributing to low zT values in this study is the low density of samples, which led to high electrical resistivity. However, our samples were prepared at the same conditions, which allowed us to study the effect of added Bi$_2$S$_3$ on the transport electronic properties of these samples regardless of their relatively high porosity.

4. Conclusion

Here, Bi$_2$Te$_{2.7}$Se$_{0.3}$ compound was systematically alloyed with Bi$_2$S$_3$ demonstrating improved thermoelectric properties, especially for multiphase compounds. In lightly alloyed samples ($x \leq 0.008$), sulfur changed the density of states and defect chemistry, significantly affecting the electrical resistivity and thermoelectric power. At higher sulfur concentrations ($x \geq 0.025$), a Bi$_2$S$_3$-based secondary phase formed and significantly improved the thermopower from -12.5 µV K^{-1} for the
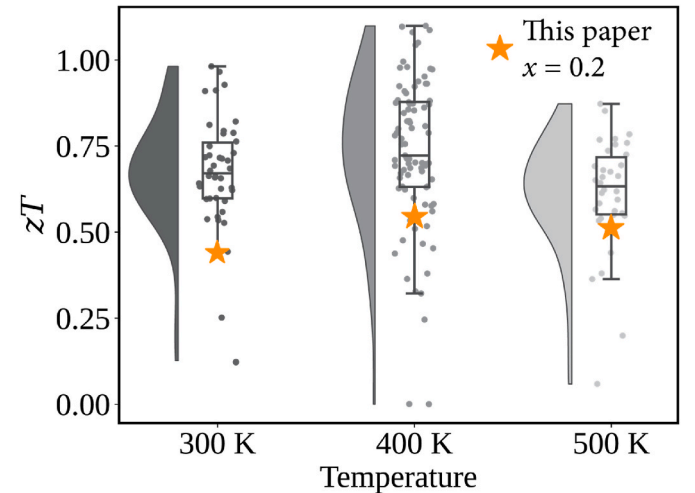

Fig. 4. Temperature dependence of zT for Bi$_2$Te$_{2.7}$Se$_{0.3}$ + xBi$_2$S$_3$, $x = $ (0, 0.003, 0.008, 0.025, 0.05, and 0.2) samples.

Fig. 5. The zT values of Bi$_2$Te$_{2.7}$Se$_{0.3}$-based samples obtained from the Starrydata open database [60] (presented in grey), compared with our sample of $Bi_2Te_{2.7}Se_{0.3}$ − 0.2 Bi_2S_3 (marked with orange stars (★)) at temperatures of 300 K, 400 K, and 500 K. Data is shown as a raincloud plot, showing the raw data, calculated boxplots, and estimated density distributions.

sulfur-free sample to $-173.9\ \mu V\ K^{-1}$ for $x = 0.025$, likely due to impurity band formation at phase interfaces. This secondary phase also effectively reduced the thermal conductivity, with the $x = 0.2$ sample reaching a remarkably low lattice thermal conductivity of $\sim 0.3\ W\ m^{-1}$ K^{-1} at 525 K, approaching the theoretical minimum of Bi_2Te_3. Overall, sulfur alloying successfully reduced thermal conductivity while increasing thermal performance in both single-phase and multi-phase samples, achieving a maximum zT of 0.55 for $x = 0.2$ compared to ~ 0.05 for the sulfur-free sample.

These results highlight the potential of isovalent sulfur substitution and secondary phase formation as promising strategies to improve Bi_2Te_3-based thermoelectric materials, potentially leading to more efficient devices for waste heat recovery and cooling applications.

CRediT authorship contribution statement

Raphael Fortulan: Writing – original draft, Visualization, Validation, Software, Investigation, Formal analysis, Data curation. **Adam Brown:** Investigation, Data curation. **Illia Serhiienko:** Writing – review & editing, Investigation, Data curation. **Takao Mori:** Writing – review & editing, Funding acquisition. **Sima Aminorroya Yamini:** Writing – review & editing, Validation, Supervision, Resources, Project administration, Methodology, Investigation, Funding acquisition, Conceptualization.

Declaration of competing interest

The authors declare the following financial interests/personal relationships which may be considered as potential competing interests: Sima Aminorroaya Yamini reports financial support was provided by Henry Royce Institute for Advanced Materials,. Takao Mori reports financial support was provided by JST Mirai Program Grant Numbers JPMJMI19A1. Illias Serhiienko reports financial support was provided by JST SPRING, Grant Number JPMJSP2124. Sima Aminorroaya Yamini reports financial support was provided by Europe Horizons. If there are other authors, they declare that they have no known competing financial interests or personal relationships that could have appeared to influence the work reported in this paper.

Data availability

Data will be made available on request.

Appendix A. Supplementary data

Supplementary data to this article can be found online at https://doi.org/10.1016/j.physb.2024.416299.

References

[1] N.S. Chauhan, S.V. Pyrlin, O.I. Lebedev, L.S.A. Marques, M.M.D. Ramos, T. Maiti, K. Kovnir, B.A. Korgel, Y.V. Kolen'ko, Compositional fluctuations mediated by excess tellurium in bismuth antimony telluride nanocomposites yield high thermoelectric performance, J. Phys. Chem. C 125 (2021) 20184–20194, https://doi.org/10.1021/acs.jpcc.1c05375.

[2] P. Gehring Devender, A. Gaul, A. Hoyer, K. Vaklinova, R.J. Mehta, M. Burghard, T. Borca-Tasciuc, D.J. Singh, K. Kern, G. Ramanath, Harnessing topological band effects in bismuth telluride selenide for large enhancements in thermoelectric properties through isovalent doping, Adv. Mater. 28 (2016) 6436–6441, https://doi.org/10.1002/adma.201601256.

[3] I.T. Witting, F. Ricci, T.C. Chasapis, G. Hautier, G.J. Snyder, The thermoelectric properties of n-type bismuth telluride: bismuth selenide alloys Bi2Te3−xSex, Research 2020 (2020) 1–15, https://doi.org/10.34133/2020/4361703.

[4] A.M. Adam, A.K. Diab, M. Ataalla, M.F. Alotaibi, A.N. Alharbi, E.M. Elsehly, Optimized thermoelectric performance in thin (Bi2Se3)1−x(Bi2Te3)x alloyed films, J. Alloys Compd. 898 (2022) 162888, https://doi.org/10.1016/j.jallcom.2021.162888.

[5] A.M. Adam, E.M.M. Ibrahim, L.V. Panina, P. Petkov, Optical and thermoelectric properties of nanocrystalline Bi2(Se1-xTex)3 films, nanoscale microscale thermophys, Eng 22 (2018) 21–38, https://doi.org/10.1080/15567265.2017.1363835.

[6] A.M. Adam, E. Lilov, P. Petkov, Optical and thermoelectric properties of nanoparticles based Bi2(Te1−xSex)3 thin films, Superlattices Microstruct 101 (2017) 609–624, https://doi.org/10.1016/j.spmi.2016.09.034.

[7] E.Kh Shokr, E.M.M. Ibrahim, A.M. Abdel Hakeem, A.M. Adam, Structural, electrical, and thermoelectrical properties of (Bi1 − xSbx)2Se3 alloys prepared by a conventional melting technique, J. Exp. Theor. Phys. 116 (2013) 166–172, https://doi.org/10.1134/S1063776113020064.

[8] X. Wu, Z. Wang, R. Jiang, Y. Tian, Y. Liu, J. Shi, W. Zhao, R. Xiong, Enhanced thermoelectric performance of p-type Bi2Te3-based materials by suppressing bipolar thermal conductivity, Mater. Today Phys. 29 (2022) 100904, https://doi.org/10.1016/j.mtphys.2022.100904.

[9] C. Zhang, Z. Peng, Z. Li, L. Yu, K.A. Khor, Q. Xiong, Controlled growth of bismuth antimony telluride BixSb2−xTe3 nanoplatelets and their bulk thermoelectric nanocomposites, Nano Energy 15 (2015) 688–696, https://doi.org/10.1016/j.nanoen.2015.05.022.

[10] B. Zhu, X. Liu, Q. Wang, Y. Qiu, Z. Shu, Z. Guo, Y. Tong, J. Cui, M. Gu, J. He, Realizing record high performance in n-type Bi2Te3-based thermoelectric materials, Energy Environ. Sci. 13 (2020) 2106–2114, https://doi.org/10.1039/D0EE01349H.

[11] M.S. Dresselhaus, G. Chen, M.Y. Tang, R.G. Yang, H. Lee, D.Z. Wang, Z.F. Ren, J.P. Fleurial, P. Gogna, New directions for low-dimensional thermoelectric materials, Adv. Mater. 19 (2007) 1043–1053, https://doi.org/10.1002/adma.200600527.

[12] D.L. Medlin, G.J. Snyder, Interfaces in bulk thermoelectric materials: a review for current opinion in colloid and interface science, Curr. Opin. Colloid Interface Sci. 14 (2009) 226–235, https://doi.org/10.1016/j.cocis.2009.05.001.

[13] M. Carle, P. Pierrat, C. Lahalle-Gravier, S. Scherrer, H. Scherrer, Transport properties of n-type Bi2(Te1−xSex)3 single crystal solid solutions (x ⩽ 0.05), J. Phys. Chem. Solid. 56 (1995) 201–209, https://doi.org/10.1016/0022-3697(94)00166-9.

[14] S.K. Mishra, S. Satpathy, O. Jepsen, Electronic structure and thermoelectric properties of bismuth telluride and bismuth selenide, J. Phys. Condens. Matter 9 (1997) 461, https://doi.org/10.1088/0953-8984/9/2/014.

[15] T. Parashchuk, R. Knura, O. Cherniushok, K.T. Wojciechowski, Ultralow lattice thermal conductivity and improved thermoelectric performance in Cl-doped Bi2Te3– xSex alloys, ACS Appl. Mater. Interfaces 14 (2022) 33567–33579, https://doi.org/10.1021/acsami.2c08686.

[16] W.-S. Liu, Q. Zhang, Y. Lan, S. Chen, X. Yan, Q. Zhang, H. Wang, D. Wang, G. Chen, Z. Ren, Thermoelectric property studies on Cu-doped n-type CuxBi2Te2.7Se0.3 nanocomposites, Adv. Energy Mater. 1 (2011) 577–587, https://doi.org/10.1002/aenm.201100149.

[17] S. Wang, H. Li, R. Lu, G. Zheng, X. Tang, Metal nanoparticle decorated n-type Bi2Te3-based materials with enhanced thermoelectric performances, Nanotechnology 24 (2013) 285702, https://doi.org/10.1088/0957-4484/24/28/285702.

[18] J.H. Kim, S.Y. Back, J.H. Yun, H.S. Lee, J.-S. Rhyee, Scattering mechanisms and suppression of bipolar diffusion effect in Bi2Te2.85Se0.15Ix compounds, Materials 14 (2021) 1564, https://doi.org/10.3390/ma14061564.

[19] J.H. Kim, H. Cho, S.Y. Back, J.H. Yun, H.S. Lee, J.-S. Rhyee, Lattice distortion and anisotropic thermoelectric properties in hot-deformed CuI-doped Bi2Te2·7Se0.3, J. Alloys Compd. 815 (2020) 152649, https://doi.org/10.1016/j.jallcom.2019.152649.

[20] J. Kennedy, P.P. Murmu, P. Kumar, G. Ramanath, Multifold enhancements in thermoelectric power factor in isovalent sulfur doped bismuth antimony telluride films, Mater. Res. Bull. 142 (2021) 111426, https://doi.org/10.1016/j.materresbull.2021.111426.

[21] K.H. Lee, H.-S. Kim, M. Kim, J.W. Roh, J.-H. Lim, W.J. Kim, S. Kim, W. Lee, Isovalent sulfur substitution to induce a simultaneous increase in the effective mass and weighted mobility of a p-type Bi-Sb-Te alloy: an approach to enhance the thermoelectric performance over a wide temperature range, Acta Mater. 205 (2021) 116578, https://doi.org/10.1016/j.actamat.2020.116578.

[22] I. Malik, T. Srivastava, K.K. Surthi, C. Gayner, K.K. Kar, Enhanced thermoelectric performance of n-type Bi2Te3 alloyed with low cost and highly abundant sulfur, Mater. Chem. Phys. 255 (2020) 123598, https://doi.org/10.1016/j.matchemphys.2020.123598.

[23] H. Shi, D. Parker, M.-H. Du, D.J. Singh, Connecting thermoelectric performance and topological-insulator behavior: Bi2Te3 and Bi2Te2Se from first principles, Phys. Rev. Appl. 3 (2015) 014004, https://doi.org/10.1103/PhysRevApplied.3.014004.

[24] A. Saji, S. Ampili, S.-H. Yang, K.J. Ku, M. Elizabeth, Effects of doping, electron irradiation, H+ and He+ implantation on the thermoelectric properties of Bi2Se3

single crystals, J. Phys. Condens. Matter 17 (2005) 2873, https://doi.org/10.1088/0953-8984/17/19/005.

[25] E.J. Ahmadov, D.M. Babanly, S.Z. Imamaliyeva, D.B. Tagiev, M.B. Babanly, Thermodynamic properties of the chalcogenide phases in the Bi–Te–S system, Inorg. Mater. 57 (2021) 227–233, https://doi.org/10.1134/S0020168521030018.

[26] W. Liu, K.C. Lukas, K. McEnaney, S. Lee, Q. Zhang, C.P. Opeil, G. Chen, Z. Ren, Studies on the Bi2Te3–Bi2Se3–Bi2S3 system for mid-temperature thermoelectric energy conversion, Energy Environ. Sci. 6 (2013) 552–560, https://doi.org/10.1039/C2EE23549H.

[27] B.H. Toby, R.B. Von Dreele, GSAS-II: the genesis of a modern open-source all purpose crystallography software package, J. Appl. Crystallogr. 46 (2013) 544–549, https://doi.org/10.1107/S0021889813003531.

[28] E37 Committee, Test Method for Determining Specific Heat Capacity by Differential Scanning Calorimetry, ASTM International, n.d https://doi.org/10.1520/E1269-11R18.

[29] E. Abrahams, S.V. Kravchenko, M.P. Sarachik, Metallic behavior and related phenomena in two dimensions, Rev. Mod. Phys. 73 (2001) 251–266, https://doi.org/10.1103/RevModPhys.73.251.

[30] C.-L. Chen, T.-H. Wang, Z.-G. Yu, Y. Hutabalian, R.K. Vankayala, C.-C. Chen, W.-P. Hsieh, H.-T. Jeng, D.-H. Wei, Y.-Y. Chen, Modulation doping enables ultrahigh power factor and thermoelectric ZT in n-type Bi2Te2.7Se0.3, Adv. Sci. 9 (2022) 2201353, https://doi.org/10.1002/advs.202201353.

[31] D. Li, J.M. Li, J.C. Li, Y.S. Wang, J. Zhang, X.Y. Qin, Y. Cao, Y.S. Li, G.D. Tang, High thermoelectric performance of n-type BiTe2.7Se0.3 via nanostructure engineering, J. Mater. Chem. A 6 (2018) 9642–9649, https://doi.org/10.1039/C8TA00525G.

[32] A. Soni, Z. Yanyuan, Y. Ligen, M.K.K. Aik, M.S. Dresselhaus, Q. Xiong, Enhanced thermoelectric properties of solution grown Bi2Te3–xSex nanoplatelet composites, Nano Lett. 12 (2012) 1203–1209, https://doi.org/10.1021/nl2034859.

[33] B. Du, J. Su, M. Tian, T. Han, J. Li, Understanding trap effects on electrical treeing phenomena in EPDM/POSS composites, Sci. Rep. 8 (2018) 8481, https://doi.org/10.1038/s41598-018-26773-y.

[34] J. Navrátil, Z. Starý, T. Plechacek, Thermoelectric properties of p-type antimony bismuth telluride alloys prepared by cold pressing, Mater. Res. Bull. 31 (1996) 1559–1566, https://doi.org/10.1016/S0025-5408(96)00149-3.

[35] Q. Zhang, B. Gu, Y. Wu, T. Zhu, T. Fang, Y. Yang, J. Liu, B. Ye, X. Zhao, Evolution of the intrinsic point defects in bismuth telluride-based thermoelectric materials, ACS Appl. Mater. Interfaces 11 (2019) 41424–41431, https://doi.org/10.1021/acsami.9b15198.

[36] F.A. Kröger, H.J. Vink, Relations between the concentrations of imperfections in crystalline solids, in: Solid State Phys., Elsevier, 1956, pp. 307–435, https://doi.org/10.1016/S0081-1947(08)60135-6.

[37] W.M. Haynes (Ed.), CRC Handbook of Chemistry and Physics, 0 ed., CRC Press, 2014 https://doi.org/10.1201/b17118.

[38] F. Habashi, Bismuth, physical and chemical properties, in: R.H. Kretsinger, V. N. Uversky, E.A. Permyakov (Eds.), Encycl. Met, Springer, New York, NY, 2013, pp. 283–284, https://doi.org/10.1007/978-1-4614-1533-6_413.

[39] H. Fang, J.-H. Bahk, T. Feng, Z. Cheng, A.M.S. Mohammed, X. Wang, X. Ruan, A. Shakouri, Y. Wu, Thermoelectric properties of solution-synthesized n-type Bi2Te3 nanocomposites modulated by Se: an experimental and theoretical study, Nano Res. 9 (2016) 117–127, https://doi.org/10.1007/s12274-015-0892-x.

[40] P. Lošťák, Č. Drašar, D. Bachan, L. Beneš, A. Krejčová, Defects in Bi2Te3−xSex single crystals, Radiat. Eff. Defect Solid 165 (2010) 211–215, https://doi.org/10.1080/10420151003616663.

[41] R.J. Mehta, Y. Zhang, C. Karthik, B. Singh, R.W. Siegel, T. Borca-Tasciuc, G. Ramanath, A new class of doped nanobulk high-figure-of-merit thermoelectrics by scalable bottom-up assembly, Nat. Mater. 11 (2012) 233–240, https://doi.org/10.1038/nmat3213.

[42] N. Xin, Y. Li, H. Shen, L. Shen, G. Tang, Realizing high thermoelectric performance in hot-pressed polycrystalline AlxSn1-xSe through band engineering tuning, J. Materiomics 8 (2022) 475–488, https://doi.org/10.1016/j.jmat.2021.06.010.

[43] Y. You, X. Su, W. Liu, Y. Yan, T. Hu, C. Uher, X. Tang, Modification of the intermediate band and thermoelectric properties in Se-doped CoSbS1−xSex compounds, RSC Adv. 7 (2017) 34466–34472, https://doi.org/10.1039/C7RA05609E.

[44] M. Jonson, G.D. Mahan, Mott's formula for the thermopower and the Wiedemann-Franz law, Phys. Rev. B 21 (1980) 4223–4229, https://doi.org/10.1103/PhysRevB.21.4223.

[45] Y.Z. Pei, Z.M. Gibbs, A. Gloskovskii, B. Balke, W.G. Zeier, G.J. Snyder, Optimum carrier concentration in n-type PbTe thermoelectrics, Adv. Energy Mater. 4 (2014) 1400486, https://doi.org/10.1002/aenm.201400486.

[46] S. Wang, J. Yang, T. Toll, J. Yang, W. Zhang, X. Tang, Conductivity-limiting bipolar thermal conductivity in semiconductors, Sci. Rep. 5 (2015) 10136, https://doi.org/10.1038/srep10136.

[47] Z. Zhang, W. Zhao, W. Zhu, S. Ma, C. Li, X. Mu, P. Wei, X. Nie, Q. Zhang, W. Zhao, Preparation and thermoelectric performance of BaTiO3/Bi0.5Sb1.5Te3 composite materials, J. Electron. Mater. 49 (2020) 2794–2801, https://doi.org/10.1007/s11664-019-07851-x.

[48] D.R. Clarke, Materials selection guidelines for low thermal conductivity thermal barrier coatings, Surf. Coat. Technol. 163–164 (2003) 67–74, https://doi.org/10.1016/S0257-8972(02)00593-5.

[49] J.A. Perez-Taborda, M. Muñoz Rojo, J. Maiz, N. Neophytou, M. Martin-Gonzalez, Ultra-low thermal conductivities in large-area Si-Ge nanomeshes for thermoelectric applications, Sci. Rep. 6 (2016) 32778, https://doi.org/10.1038/srep32778.

[50] A. Banik, B. Vishal, S. Perumal, R. Datta, K. Biswas, The origin of low thermal conductivity in Sn 1− x Sb x Te: phonon scattering via layered intergrowth nanostructures, Energy Environ. Sci. 9 (2016) 2011–2019.

[51] A.U. Khan, K. Kobayashi, D.-M. Tang, Y. Yamauchi, K. Hasegawa, M. Mitome, Y. Xue, B. Jiang, K. Tsuchiya, D. Golberg, Y. Bando, T. Mori, Nano-micro-porous skutterudites with 100% enhancement in ZT for high performance thermoelectricity, Nano Energy 31 (2017) 152–159, https://doi.org/10.1016/j.nanoen.2016.11.016.

[52] S. Li, X. Liu, Y. Liu, F. Liu, J. Luo, F. Pan, Optimized hetero-interfaces by tuning 2D SnS2 thickness in Bi2Te2.7Se0.3/SnS2 nanocomposites to enhance thermoelectric performance, Nano Energy 39 (2017) 297–305, https://doi.org/10.1016/j.nanoen.2017.07.011.

[53] J. Zhang, H. Ming, D. Li, X. Qin, J. Zhang, L. Huang, C. Song, L. Wang, Ultralow thermal conductivity and high thermoelectric performance of N-type Bi2Te2.7Se0.3-based composites incorporated with GaAs nanoinclusions, ACS Appl. Mater. Interfaces 12 (2020) 37155–37163, https://doi.org/10.1021/acsami.0c09338.

[54] B. Jabar, X. Qin, A. Mansoor, H. Ming, L. Huang, M.H. Danish, J. Zhang, D. Li, C. Zhu, H. Xin, C. Song, Enhanced power factor and thermoelectric performance for n-type Bi2Te2.7Se0.3 based composites incorporated with 3D topological insulator nanoinclusions, Nano Energy 80 (2021) 105512, https://doi.org/10.1016/j.nanoen.2020.105512.

[55] Y.-K. Zhu, J. Guo, Y.-X. Zhang, J.-F. Cai, L. Chen, H. Liang, S.-W. Gu, J. Feng, Z.-H. Ge, Ultralow lattice thermal conductivity and enhanced power generation efficiency realized in Bi2Te2.7Se0.3/Bi2S3 nanocomposites, Acta Mater. 218 (2021) 117230, https://doi.org/10.1016/j.actamat.2021.117230.

[56] S. Li, Y. Liu, F. Liu, D. He, J. He, J. Luo, Y. Xiao, F. Pan, Effective atomic interface engineering in Bi2Te2.7Se0.3 thermoelectric material by atomic-layer-deposition approach, Nano Energy 49 (2018) 257–266, https://doi.org/10.1016/j.nanoen.2018.04.047.

[57] D.H. Kim, H.-S. Kim, S. Hong, J.H. Lee, J.G. Han, H.S. Cho, S.W. Lee, S.-I. Kim, Investigation of PdTe2 phase segregation on thermoelectric properties of n-type Bi2Te2.7Se0.3 fabricated by melt-spinning technique for possible carrier filtering effect, Electron. Mater. Lett. 17 (2021) 436–442, https://doi.org/10.1007/s13391-021-00300-0.

[58] Q. Hu, W. Qiu, L. Chen, J. Chen, L. Yang, J. Tang, Realize high thermoelectric properties in n-type Bi2Te2.7Se0.3/Y2O3 nanocomposites by constructing heterointerfaces, ACS Appl. Mater. Interfaces 13 (2021) 38526–38533, https://doi.org/10.1021/acsami.1c12722.

[59] S.F. Ma, C.C. Li, L. Xing, X. Mu, W.T. Zhu, X.L. Nie, X.H. Sang, P. Wei, Q.J. Zhang, W.Y. Zhao, Effects of Ni magnetic nanoparticles on thermoelectric properties of n-type Bi2Te2.7Se0.3 materials, J. Electron. Mater. 49 (2020) 2881–2889, https://doi.org/10.1007/s11664-020-07956-8.

[60] Y. Katsura, M. Kumagai, T. Kodani, M. Kaneshige, Y. Ando, S. Gunji, Y. Imai, H. Ouchi, K. Tobita, K. Kimura, K. Tsuda, Data-driven analysis of electron relaxation times in PbTe-type thermoelectric materials, Sci. Technol. Adv. Mater. 20 (2019) 511–520, https://doi.org/10.1080/14686996.2019.1603885.